Model Treatment of Tensile Deformation of Semicrystalline Polymers: Static Elastic Moduli and Creep Parameters Derived for a Sample of Polyethylene

K. Hong, A. Rastogi, and G. Strobl*

Physikalisches Institut, Albert-Ludwigs-Universität, 79104 Freiburg, Germany

Received April 28, 2004; Revised Manuscript Received October 19, 2004

ABSTRACT: A model constructed to treat tensile deformation of semicrystalline polymers introduced in a first paper is again applied to measurements on poly(ethylene-*co*-12% vinyl acetate) and is now used for an extraction of true elastic moduli and a discussion of the creep behavior. Elastic moduli vary in a characteristic manner during the stretching. There is first a decrease, with a maximum decay at the yield point, followed by an increase setting in with the formation of fibrils. Creep kinetics obey after a short initial period a log t law, which is reproduced by the model. A relation between creep and stress relation predicted by the model is confirmed by the experiments at lower strains.

1. Introduction

The stress arising during stretching a semicrystalline polymer is made up of three different contributions: (1) rubberlike forces originating from the stretched network of entangled amorphous chains, (2) forces transmitted by the skeleton of crystallites, and (3) the forces arising from the viscosity. A tensile deformation changes the structure of the skeleton of crystallites, both as a change in their texture, i.e., their orientational distribution, and as a change of their coupling. In addition, the crystal blocks which made up the skeleton can be sheared and also completely destroyed and transformed into fibrils. These structural changes are partly reversible, i.e., are removed again on unloading the sample, and partly irreversible, i.e., are permanent for normal experimental time scales. After various investigations on different systems,[1−3] we carried out a comprehensive series of measurements on a sample of low-crystallinity polyethylene.[4] On the basis of the results, a model was constructed which is able to describe all observations. Experiments indicate that in the limit of a zero strain rate, where all viscous forces vanish, one finds in addition to the network force also a nonvanishing force transmitted by the crystal skeleton. The model correspondingly describes the total measured stress as a sum of a quasi-static stress based on network and crystallites plus viscous forces. It is depicted in Figure 1, having three branches with stresses $\phi_c\sigma_c$, $(1 - \phi_c)\sigma_n$, and σ_r, related to the crystal skeleton (volume fraction ϕ_c), the deformed network (volume fraction $1 - \phi_c$), and the relaxing viscous stress, respectively. The two lower branches determine together the quasi-static stress−strain relationship. The model assumes a homogeneous strain. This is suggested by the existence of critical strains—true strains ϵ_H(A), ϵ_H(B), and ϵ_H(C) where the deformation mechanism changes—which are independent of the crystallinity. All model parameters could be derived for the investigated sample. In particular, the properties of the relaxing branch followed from stress relaxation experiments exclusively. The properties of the crystallite branch, which is made up of two elements representing the recoverable elastic and a nonrecoverable plastic strain, were derived from step-cycle tests, i.e., a stepwise stretching interrupted by unloading−loading cycles. To decompose the quasi-static stress into its two components $\phi_c\sigma_c$ and $(1 - \phi_c)\sigma_n$, we evaluated the asymptotic behavior for large strains which is dominated by the network forces. This allowed a determination of the associated network shear modulus G.

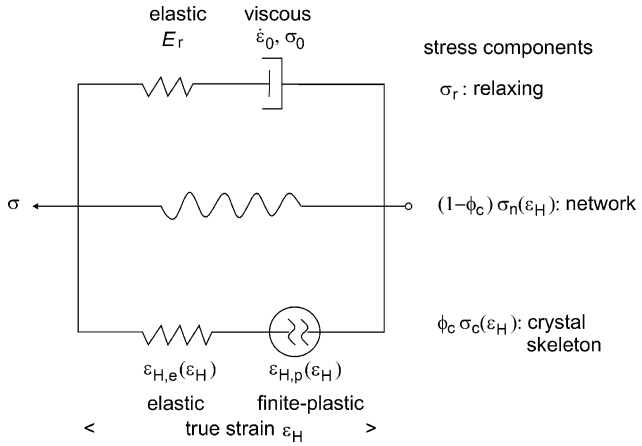

Figure 1. A three-component model treating tensile deformation of semicrystalline polymers.

The model now being specified, it allows to treat more experiments and give answers to more questions. In this second paper two points will be addressed:

(i) Elastic moduli as measured at the beginning of drawing or also for preoriented samples are always modified by the presence of viscous forces. The model provides via the quasi-static stress−strain relationship the purely elastic contributions. As will be shown in the following, this elastic contribution, i.e., the true elastic modulus, shows remarkably strong changes.

(ii) The model allows to treat also results of creep experiments. One expects certain relationships between the results of creep and stress relaxation measurements which can be checked.

The creep experiments presented and discussed in this paper were again carried out with an Instron 4301 tensile stretching machine run with self-developed programs. The sample was the same as previously, a commercial poly(ethylene-*co*-vinyl acetate) with 12 wt % counits.

10.1021/ma049172x CCC: $27.50
Published on Web 11/26/2004

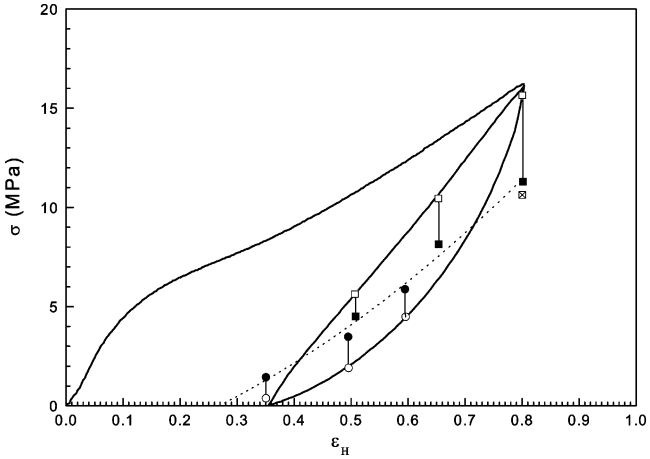

Figure 2. PEVA12: unloading−loading cycle run after stretching to $\epsilon_H = 0.8$ with a strain rate $\dot{\epsilon}_H = 0.005\ s^{-1}$. Elastic stress−strain dependence in the zero strain rate limit set up by the relaxed stresses (dotted line).

2. Results and Discussion

2.1. Stiffness Variations on Stretching. The experiment presented in Figure 2 shows the effect of the viscous forces on the stresses measured during a stretching followed by an unloading−reloading cycle. At first, the sample is stretched up to a true strain $\epsilon_H = 0.8$ with a strain rate $\dot{\epsilon}_H = 0.005\ s^{-1}$, then it is unloaded until the stress vanishes, and finally it is reloaded again, up to the stress which was originally reached on the initial stretching curve. The unloading−reloading cycle represents a reversible process which, as is demonstrated by the stress difference between the unloading and the reloading part, is affected by the presence of viscous forces. The figure shows what can be done in order to obtain the true elastic stiffness of this predrawn sample: All the points with filled symbols included in the figure were obtained when the stresses reached along the circle were allowed to relax completely. As shown by the direction of change, stress relaxation can take place in two ways: either by a decrease or an increase of the initial stresses. Both together, the relaxed stresses measured during the unloading with changes in upward direction and the relaxed stresses measured during the reloading with changes in downward direction define together the stress−strain dependence which would be measured in the limit of zero strain rates. The dotted line therefore represents the true, purely elastic stress−strain relationship of the predrawn sample; its slope gives the associated true elastic modulus. The point where the true stress vanishes in the zero strain rate limit determines the true plastic strain introduced into the sample by stretching it at first to $\epsilon_H = 0.8$. The experiment provides in this way a decomposition of the imposed strain in its two basic parts: a plastic strain and an elastic strain.

Figure 3 taken from the first paper of this series[4] shows the complete true stress−strain curve obtained for a strain rate $\dot{\epsilon}_H = 0.005\ s^{-1}$ together with the true stress−strain dependence which would be measured in the limit of zero strain rates. The points setting up the latter dependence, denoted $\phi_c\sigma_c + (1 - \phi_c)\sigma_n$, were obtained by stress relaxation experiments at the indicated imposed strains. Figure 4, again taken from ref 4, collects the results of experiments carried out to determine for various imposed strains the plastic and the elastic parts. The quasi-static stress−strain relationship from Figure 3 together with the decomposition of the strain shown in Figure 4 allows to construct Figure 5. The dotted lines in this figure represent the true elastic responses of samples drawn to various strains, i.e., the elastic responses which would be measured in the limit of zero strain rates. The straight lines connect the two end points of curves like the one

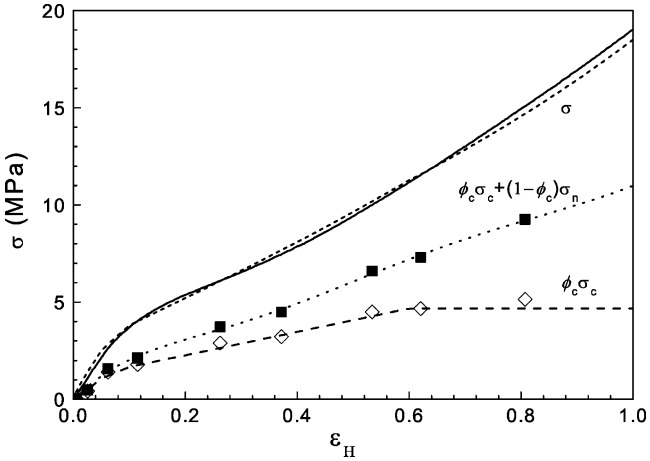

Figure 3. Stretching curve $\sigma(\epsilon_H)$ measured for a strain rate $\dot{\epsilon}_H = 0.005\ s^{-1}$, quasi-static stress−strain dependence $(\phi_c\sigma_c + (1 - \phi_c)\sigma_n)(\epsilon_H)$, and elasto-plastic contribution of the crystal skeleton $(\phi_c\sigma_c)$.

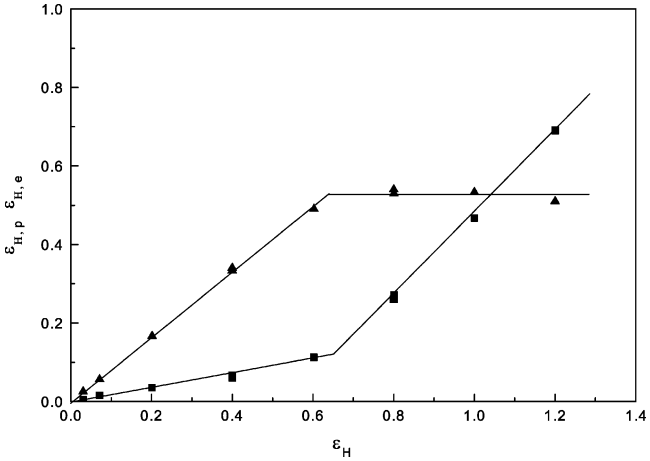

Figure 4. PEVA12: plastic (squares) and elastic (triangles) parts of the total strain in the zero strain rate limit.

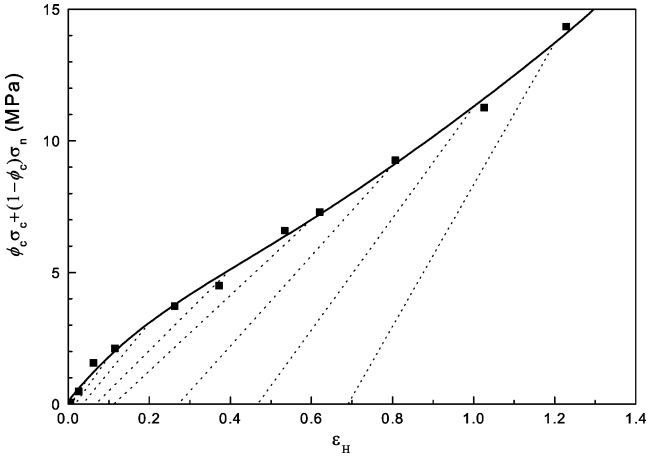

Figure 5. Hypothetical result of a step-cycle experiment in the zero strain rate limit: Quasi-static stress−strain dependence and elastic unloading/loading curves at different strains as obtained using the results of Figures 3 and 4.

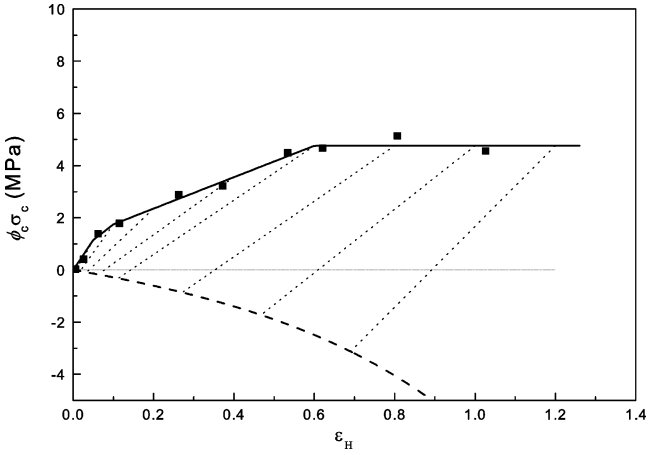

Figure 6. Quasi-static stress−strain relationship $\phi_c\sigma_c(\epsilon_H)$ for the crystal skeleton and associated elastic unloading/loading curves at different strains. A compressive skeleton stress and the network stress compensate each other in the stress-free end state.

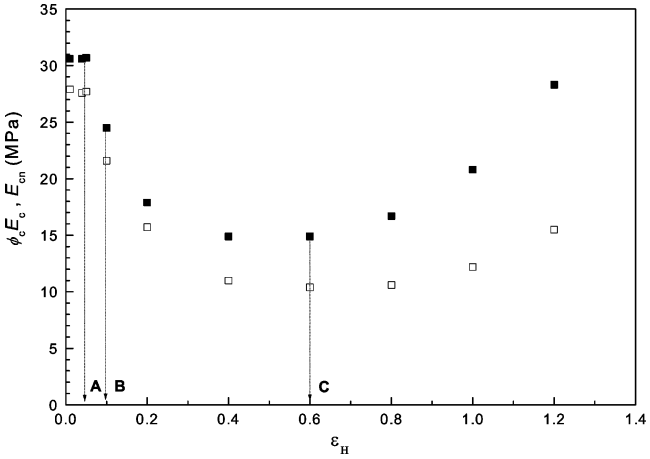

Figure 7. Variation of the elastic modulus E_{cn} (filled squares)- and the contribution of the crystal skeleton $\phi_c E_c$ (open squares) of stretched samples with the imposed strain. Data are derived from the slopes of the unloading/loading lines in Figures 5 and 6, respectively.

shown in Figure 2. We neglect their slight curvature and derive effective elastic moduli, denoted E_{cn}, from the slopes of the straight lines.

Elasticity in semicrystalline polymers arises from the contributions of both the network of entangled chains in the amorphous parts of the sample and the skeleton of coupled crystalline blocks. The crystalline skeleton can be stretched and also bent, and it is possible to obtain this contribution separately. Figure 3 shows also the strain dependence of the crystal skeleton stress $\phi_c\sigma_c$. In the limit of high strains it reaches a constant value. With the knowledge of the dependencies $\phi_c\sigma_c(\epsilon_H)$ and $\epsilon_{H,e}(\epsilon_H)$ it is possible to determine the stiffness of the skeleton of crystallites only. Figure 6 shows a corresponding drawing. The dotted lines depict the elastic responses of the skeleton of crystallites in predrawn samples. The slopes of the lines give the respective elastic moduli, denoted E_c in the following, multiplied by ϕ_c. As can be observed, the complete unloading results in a negative stress, i.e., a pressure on the crystal skeleton. It just compensates the positive stress of the amorphous network which remains stretched in the stress-free equilibrium state reached after a complete unloading.

The elastic moduli E_{cn} and $\phi_c E_c$ of samples predrawn to certain initial strains as they follow from the dotted lines in Figures 5 and 6 are collected in Figure 7. Quite interestingly, the part of the elastic modulus associated with the crystal skeleton starts with an initial value of 28 MPa but then shows a large decrease, down to about 10 MPa. Subsequently, beginning at $\epsilon_H = 0.6$, which is the location of the critical point C, the modulus begins to rise again. The decrease in the stiffness sets in at the critical point A ($\epsilon_H(A) = 0.05$) and has its largest value around point B ($\epsilon_H(B) = 0.1$). We addressed point B as the "yield point", although it is according to Figure 4 *not* associated with the onset of plastic flow. The actual reason for the strain softening is now demonstrated by Figure 7: It is due to a strong decrease in the stiffness of the crystal skeleton. This stiffness is controlled by the coupling of the blocks in the skeleton, much more than by the intrinsic Young's modulus of a single block which is in the GPa range. The sample stretching affects this coupling and obviously reduces it. In which way this happens becomes evident, for example, from a look at the electron micrographs obtained by Geil et al. for poly-

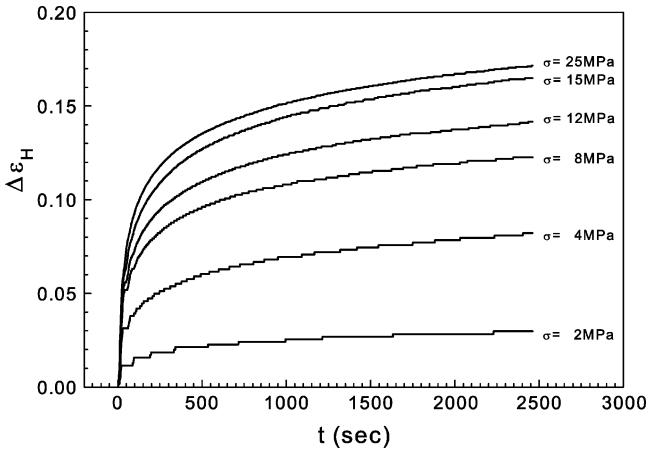

Figure 8. Creep curves measured at the indicated true stresses after a stretching with a constant strain rate $\dot{\epsilon}_H = 0.005\ s^{-1}$ to corresponding initial strains.

(1-butene).[5] The crystal blocks, being first arranged in planes to set up crystal lamellae, become separated from each other by sliding processes and thereby weaken their coupling.

2.2. Creep Behavior. Figure 8 presents several creep curves which were measured after stretching a sample with a strain rate $\dot{\epsilon}_H = 0.005\ s^{-1}$ to different points on the stretching curve and then keeping the true stress constant. A constant true stress was achieved by continuously adjusting the tensile force f acting on the sample so that the tensile stress

$$\sigma = f\lambda \quad (\lambda\text{: extension ratio})$$

is kept constant. Creep curves were thus obtained at different fixed values of σ which are indicated in the figure.

Figure 9 depicts these curves again in plots of the amount of creep $\Delta\epsilon_H$ vs log t. Interestingly, the representation shows that the creep follows after a short initial period a log t law.

Another property shows up in Figure 10. Samples were at first stretched with different strain rates (0.001, 0.003, and 0.01 s^{-1}), always to that point where a stress of $\sigma = 10$ MPa was reached. Then this stress was fixed, and the creep under this stress was observed. The figure

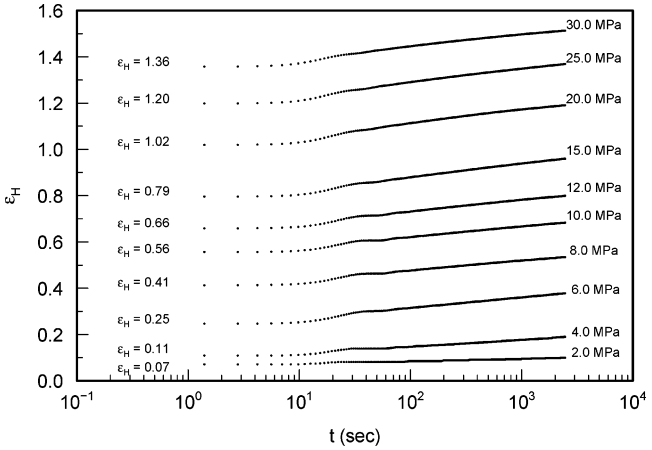

Figure 9. Same as Figure 8. Representation showing that the creep follows a log t law.

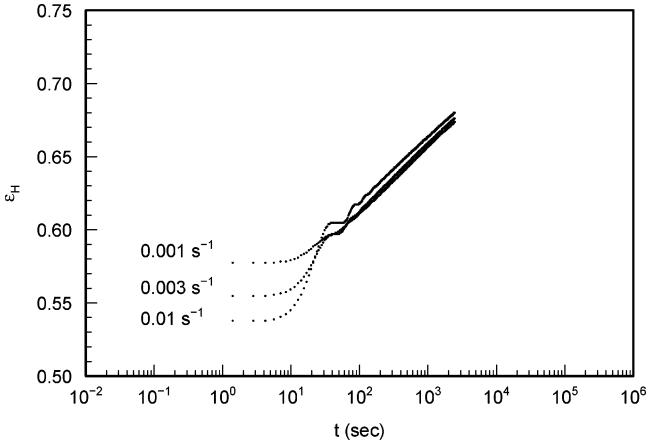

Figure 10. Creep curves measured for $\sigma = 10$ MPa after a stretching with three different strain rates to corresponding initial strains.

shows that while creep started at different initial strains, varying between 0.54 and 0.58, the curves finally coincide and follow a common time dependence. The associated law is of the log t type. The observation means that memory effects are not present, and the creep rate $d\Delta\epsilon/dt$ is a function of the applied stress σ and the momentary strain ϵ_H only.

2.2.1. Model Treatment of Creep Kinetics. The model shown in Figure 1 allows an analytical treatment of the creep. During creep the viscous force represented by the relaxing stress branch continuously decays, which is compensated by an increasing elastic stress arising from a corresponding stretching of the amorphous network and the crystal skeleton. This condition means

$$d\sigma = \phi_c\, d\sigma_c + (1 - \phi_c)\, d\sigma_n + d\sigma_r = 0 \qquad (1)$$

For the stress decay in the relaxing stress branch we write

$$\sigma_r(t) = \sigma_r(0) - \Delta\sigma(t) \qquad (2)$$

For the corresponding stress increase in the two other branches we formulate correspondingly

$$\phi_c\sigma_c(t) + (1 - \phi_c)\sigma_n(t) = \phi_c\sigma_c(0) + (1 - \phi_c)\sigma_n(0) + \Delta\sigma(t) \qquad (3)$$

using the same function $\Delta\sigma(t)$ in eqs 2 and 3. The relaxing stress branch is composed by two components: an elastic strain associated with an element with a modulus E_r and a viscous "dashpot". As was pointed out when introducing the model, viscous forces in semicrystalline and also amorphous polymer systems generally follow the Eyring equation of viscosity rather than the simple Newtonian law. For a time-dependent stress $\sigma_r(t)$ acting in the branch describing the relaxing stress this leads to a total strain rate

$$\dot{\epsilon}_H(t) = \dot{\epsilon}_0 \sinh\left(\frac{\sigma_r(0) - \Delta\sigma(t)}{\sigma_0}\right) - \frac{1}{E_r}\frac{d\Delta\sigma}{dt} \qquad (4)$$

The total amount of creep in the relaxing stress branch and simultaneously in the two other branches—the model assumes a homogeneous strain and additive stresses—follows by integration as

$$\Delta\epsilon_H(t) = \dot{\epsilon}_0 \int_0^t \sinh\left(\frac{\sigma_r(0) - \Delta\sigma(t')}{\sigma_0}\right) dt' - \frac{\Delta\sigma(t)}{E_r} \qquad (5)$$

Such a time-dependent creep produces in the branches associated with the amorphous network and the crystal skeleton an increase of the total stress of

$$\Delta\sigma(t) = \hat{E}_{cn}\Delta\epsilon_H(t) \qquad (6)$$

Here, we again write $\Delta\sigma(t)$, i.e., use the same function as for the stress decay in the relaxing stress branch; with this choice the condition of creep eq 1 is fulfilled. Equation 6 includes as a parameter the differential elastic modulus associated with the quasi-static stress–strain dependence

$$\hat{E}_{cn} = \frac{d(\phi_c\sigma_c + (1 - \phi_c)\sigma_n)}{d\epsilon_H} \qquad (7)$$

Introducing eq 6 into eq 5 and differentiating both sides leads to

$$\left(1 + \frac{\hat{E}_{cn}}{E_r}\right)\frac{d\Delta\epsilon_H}{dt} = \dot{\epsilon}_0 \sinh\left(\frac{\sigma_r(0) - \hat{E}_{cn}\Delta\epsilon_H(t)}{\sigma_0}\right) \qquad (8)$$

We choose dimensionless quantities

$$y(t) = \frac{\hat{E}_{cn}\Delta\epsilon_H(t)}{\sigma_0} \qquad (9)$$

$$y(\infty) = \frac{\sigma_r(0)}{\sigma_0} \qquad (10)$$

and the characteristic time τ_{cr}

$$\tau_{cr} = \frac{\sigma_0\left(1 + \frac{\hat{E}_{cn}}{E_r}\right)}{\dot{\epsilon}_0\hat{E}_{cn}} = \frac{\eta_0}{\hat{E}_{cn}}\left(1 + \frac{\hat{E}_{cn}}{E_r}\right) \qquad (11)$$

and then write instead of eq 8

$$\frac{dy}{dt} = \frac{1}{\tau_{cr}} \sinh(y(\infty) - y) \qquad (12)$$

This differential equation can be solved. A similar equation had to be solved when treating the stress

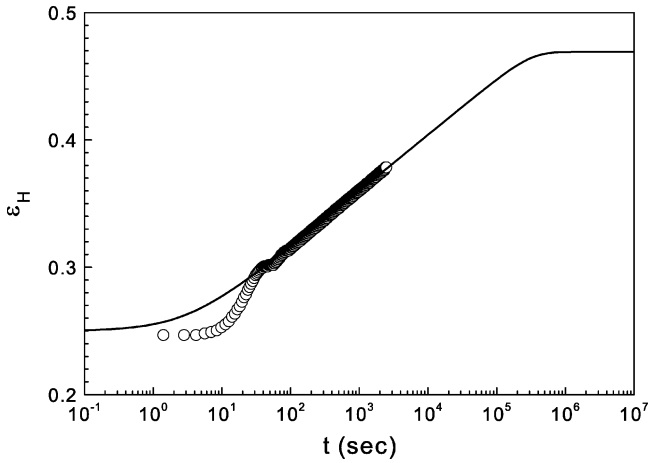

Figure 11. Same as the creep curve starting from $\epsilon_H = 0.25$ included in Figure 9, in a comparison with the model calculation.

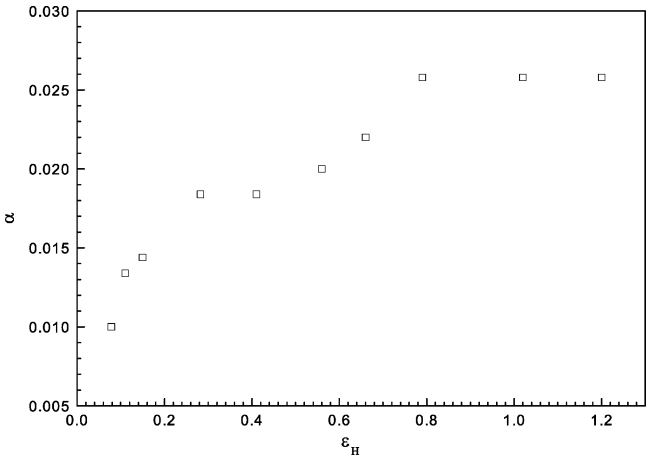

Figure 12. Variation of the slope of the creep curves in Figure 9 with the initially imposed strain (stretching with $\dot{\epsilon}_H = 0.005$ s^{-1}). The slope α controls the amount of creep and equals the ratio $\sigma_0/\hat{E}_{cn}$.

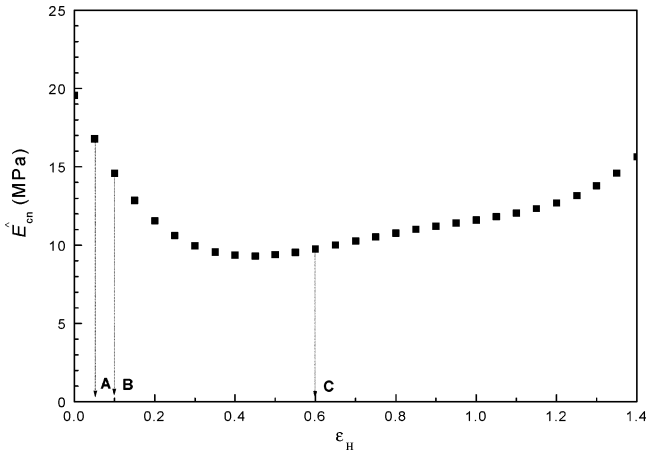

Figure 13. Differential stiffness $\hat{E}_{cn}$ along the quasi-static stress−strain curve.

relaxation experiments. The solution is given in the first paper[4] and has the form

$$y(t) = y(\infty) - 2\,\mathrm{atanh}\left[\tanh\left(\frac{y(\infty)}{2}\right)\exp\left(-\frac{t}{\tau_{cr}}\right)\right] \quad (13)$$

Since

$$\mathrm{atanh}\,x = \frac{1}{2}\ln\left(\frac{1-x}{1+x}\right) \quad (|x| < 1) \quad (14)$$

we can write for

$$\frac{t}{\tau_{cr}} \ll 1 \quad (15)$$

as an approximation

$$y(t) \approx \ln\left(\frac{t}{\tau_{cr}}\right) + \mathrm{const} \quad (16)$$

which means, using again the variables of the measurement

$$\Delta\epsilon_H(t) \approx \frac{\sigma_0}{\hat{E}_{cn}}\ln\left(\frac{t}{\tau_{cr}}\right) + \mathrm{const} \quad (17)$$

This result with a log t law agrees with the experiment. It gives us the meaning of the slope of the creep curves presented in Figure 9. The corresponding approximate expression for the stress relaxation experiment had the form[4]

$$\Delta\sigma(t) \approx \sigma_0 \ln\left(\frac{t}{\tau_r}\right) + \mathrm{const} \quad (18)$$

Equation 13 can indeed be used to represent the creep curves. Figure 11 shows this for the example of the creep started from $\epsilon_H = 0.25$ and $\sigma = 6$ MPa, after a stretching with a strain rate $\dot{\epsilon}_H = 0.005$ s^{-1} (one of the curves depicted in Figure 9). All the parameters included in eq 13, with the definitions eqs 9 and 10, are already known from the other experiments:

(i) The differential stiffness $\hat{E}_{cn}$ follows from the static stress−strain dependence shown in Figure 3 as $\hat{E}_{cn} =$ 10.5 MPa.

(ii) The total amount of stress relaxation at $\epsilon_H = 0.25$ shows up in Figure 3 as the stress difference between the measured stress−strain curve and the quasi-static stress−strain relationship and has the value 2.3 MPa.

(iii) The characteristic time constant τ_{cr} is given by eq 11. The Newtonian viscosity η_0 and the modulus E_r associated with the relaxing stress branch have been derived previously from measured stress−strain curves together with the results of the stress-relaxation experiments. The values are $\eta_0 = 1.4 \times 10^6$ MPa s and $E_r =$ 90 MPa.

This leads to $\tau_{cr} = 1.5 \times 10^5$ s. We now keep the value of the reference stress σ_0 open and determine it by the adjustment of eq 13 to the measured curve. The curve shown in the figure was obtained for $\sigma_0 = 0.2$ MPa. σ_0 was also directly derived from the stress relaxation experiments, with the result $\sigma_0 = 0.23$ MPa. This can be considered as a good agreement.

The agreement is less satisfactory at higher strains and stresses. According to eq 17, the slope of the creep curve yields the ratio $\sigma_0/\hat{E}_c$. All the slopes measured in creep experiments starting from different points along the stress−strain curve are collected in Figure 12. Figure 13 presents in addition the differential moduli $\hat{E}_{cn}$ derived from the static stress−strain curve. After the initial decrease, leading to a minimum at around

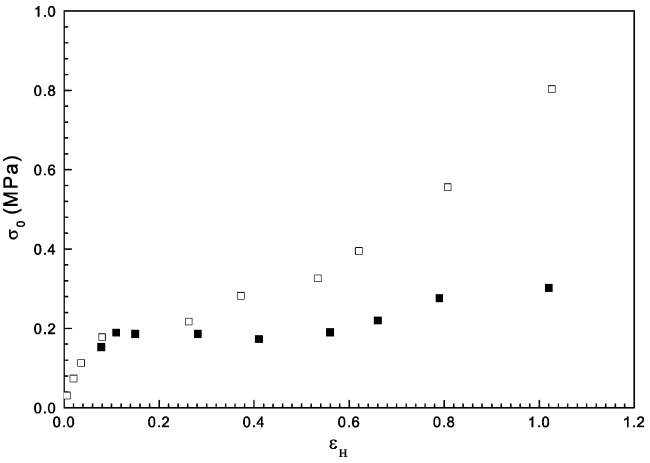

Figure 14. Checking the relationship between creep and relaxation curves: reference stresses $\sigma_0(\epsilon_H)$ derived from the creep curves (filled symbols) and the stress relaxation curves (open symbols) in comparison.

$\epsilon_H = 0.4$, its value increases only slowly. According to eq 17, a multiplication of the curve shown in Figure 12 with $\hat{E}_{cn}(\epsilon_H)$, as given in Figure 13, yields the reference stress σ_0. Figure 14 shows all the values thus obtained in a comparison with the values derived from the stress relaxation experiments. While the agreement is satisfactory at low strains, a difference shows up at higher strains. One reason can be given: In the model treatment the reference stress σ_0 was used as a constant, which is incorrect. Figure 14, taken from ref 4, indicates a continuous increase with the strain. In principle, this variation could be accounted for in the solution of the differential equation (12). However, then the equation can only be solved by numerical means and loses its transparency.

3. Conclusion

Elastic moduli of semicrystalline polymers derived from slopes in stress−strain curves are generally apparent values which include nonnegligible contributions of viscous forces. We use a previously introduced model describing the development of stress during uniaxial tensile deformations in order to determine true elastic moduli in a sample of P(E-*co*-VA). Following the variation during stretching shows that the strain softening observed at the yield point originates from a strong decrease in the true elastic modulus rather than an onset of plastic flow. The fibril formation at higher strains shows up as a stiffness increase. It is also shown that the model describes correctly the creep kinetics and allows to discuss relationships between the kinetics of creep and stress relaxation.

Acknowledgment. Support of this work by the Deutsche Forschungsgemeinschaft (Sonderforschungsbereich 428) is gratefully acknowledged. Thanks are also due to the "Fonds der Chemischen Industrie" for financial help. We greatly appreciate the advice in numerical works given by Werner Stille.

References and Notes

(1) Hiss, R.; Hobeika, S.; Lynn, C.; Strobl, G. *Macromolecules* **1999**, *32*, 4390.
(2) Men, Y.; Strobl, G. *J. Macromol. Sci., Phys.* **2001**, *B40*, 775.
(3) Al-Hussein, M.; Strobl, G. *Macromolecules* **2002**, *35*, 8515.
(4) Hong, K.; Rastogi, A.; Strobl, G. *Macromolecules* **2005**, *38*, 10165.
(5) Yang, Y. C.; Geil, P. H. *Makromol. Chem.* **1985**, *186*, 1961.

MA049172X